AMERICAN SOCIETY of
GENE & CELL
THERAPY

The Vascular Disrupting Agent CA4P Improves the Antitumor Efficacy of CAR-T Cells in Preclinical Models of Solid Human Tumors

Changwen Deng,[1,4] Jingjing Zhao,[1,4] Shixin Zhou,[1] Jiebin Dong,[1] Jixiang Cao,[1] Junshuang Gao,[1] Yun Bai,[1] and Hongkui Deng[1,2,3]

[1]Department of Cell Biology and Stem Cell Research Center, School of Basic Medical Sciences, State Key Laboratory of Natural and Biomimetic Drugs, Peking University Health Science Center, Peking University, Beijing 100191, China; [2]MOE Key Laboratory of Cell Proliferation and Differentiation, College of Life Sciences, Peking-Tsinghua Center for Life Sciences, Peking University, Beijing 100191, China; [3]Shenzhen Stem Cell Engineering Laboratory, Key Laboratory of Chemical Genomics, Peking University Shenzhen Graduate School, Shenzhen 518055, China

Chimeric antigen receptor (CAR) T cell therapy remains relatively ineffective against solid tumors due to inadequate infiltration and *in vivo* expansion of CAR-T cells. Unlike hematological malignancies, solid tumors have vascular barriers that hinder CAR-T cells from reaching the tumor site. Here, we demonstrated that combretastatin A-4 phosphate (CA4P), a vascular disrupting agent (VDA), can significantly improve the infiltration ability of CAR-T cells in solid tumors as evidenced by elevated levels of IFN-γ. Moreover, combined treatment with CA4P and CAR-T cells greatly increased the therapeutic efficiency of the CAR-T cells in subcutaneous ovarian cancer mouse xenograft models and patient-derived xenograft (PDX) models of colon and ovarian carcinoma. Our findings highlight CA4P as an effective antitumor agent candidate for combination with CAR-T cells in clinical applications to treat solid tumors.

INTRODUCTION

Chimeric antigen receptor (CAR)-T cells are T cells that have been genetically engineered to express a receptor recognizing a specific antigen that confers specific cytotoxicity against malignant cells bearing the same tumor antigen.[1] Recently, CAR-T cell therapy has rapidly advanced into a promising therapeutic approach for hematological malignancies, including lymphomas. Notably, autologous CAR-T cell therapy specific for the CD19 B lymphocyte molecule has recently been approved by the US Food and Drug Administration (FDA), and this approach produces significant beneficial responses in patients with multiple myeloma or acute lymphoblastic leukemia.[2–4] Despite its success in hematological cancer treatment, CAR-T cell therapy still faces multiple hurdles as a treatment for solid tumors, the major type of cancer.

One of the important factors affecting the treatment of solid tumors with CAR-T cells, at least in part, is the restricted accumulation and survival of transferred CAR-T cells in the tumor site.[5–9] The physical barriers in a tumor site, such as the vascular barriers, lead to an abnormal vascular bed and matrix in the tumor, which are an important reason why CAR-T cells have difficulties entering the tumor site.[10] New blood vessels are required to maintain ongoing exponential growth depending on the type of tumor and its related microenvironment, especially the hypoxic and acidic zones of the microenvironment.[11,12] The irregular shape and diameter of a tumor as well as the unstable pericyte coverage of tumor blood vessels can produce an abnormal vascular network, which further aggravates hypoxia and acidification. The consequent microenvironmental dysbiosis and disorder of the extracellular matrix largely obstruct the infiltration of antitumor lymphocytes into the tumor tissue.[13,14] Therefore, developing approaches to destroy the existing vascular network and prevent neovascularization in solid tumors seems to be a feasible way to promote the infiltration of CAR-T cells into solid tumor sites.

Antiangiogenic drugs such as vascular disrupting agents (VDAs) have shown great potential in disrupting the vascular microenvironment in solid tumors. VDAs induce apoptosis in tumor cell-associated vascular endothelial cells by affecting the microtubule polymerization stability of these cells, which then causes damage to the vascular system and reduces the intratumoral blood supply to cause tumor cell necrosis in the tumor tissue.[15,16] Therefore, it is of interest to test whether VDAs can promote the infiltration of CAR-T cells into solid tumors and enhance the therapeutic efficiency of CAR-T cells.
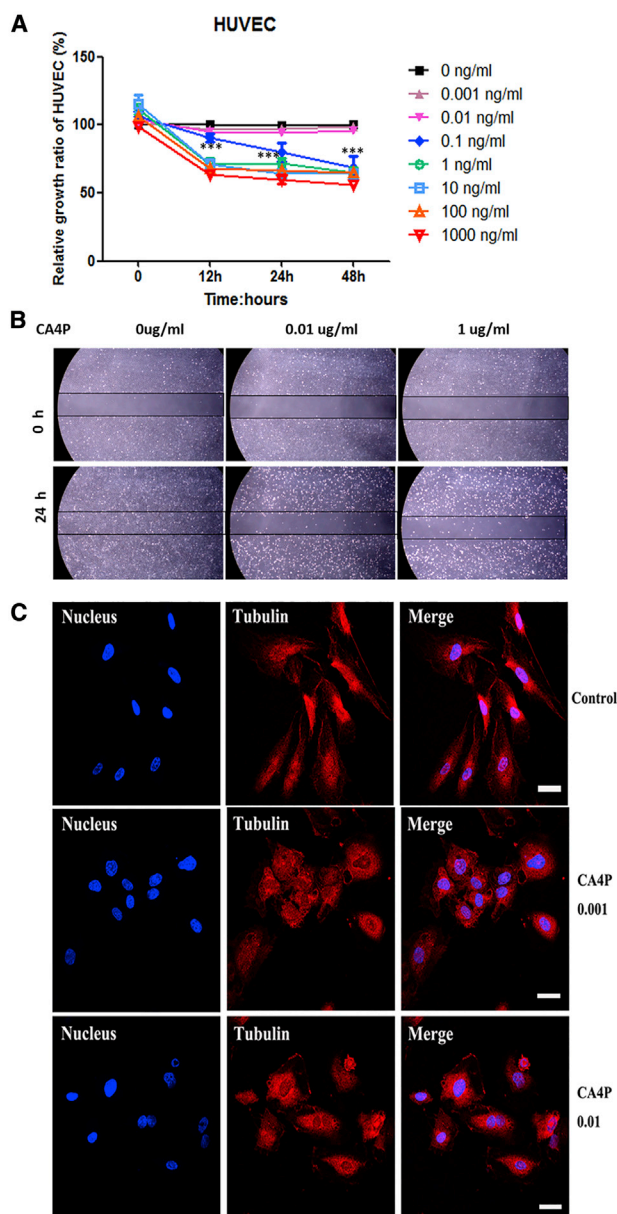
Figure 1. Effect of CA4P on Vascular Endothelial Cells

(A) CA4P inhibits HUVEC proliferation. HUVECs were seeded at a density of 2×10^4 cells in each well of 96-well plates and cultured overnight, with CA4P added at different concentrations. The proliferation of the cells was measured using a cell counting kit-8 (CCK8) assay at the indicated time points. The absorbance of each well was measured with a microplate reader at dual wavelengths of 450 nm and 690 nm. All experiments were performed three times, and the results are presented as the mean ± SD (ns, no significance; *p < 0.05; **p < 0.01; and ***p < 0.001; n ≥ 3). (B) CA4P inhibits HUVEC migration. The effect of CA4P on the migration of HUVECs was observed by a wound-healing assay. A lesion was produced across a HUVEC monolayer, and HUVEC monolayers were incubated with different doses of CA4P (0.01 µg/mL, 1 µg/mL, and control) for 24 h and then photographed. A representative image is shown. Original magnification, ×4. Scale bar, 500 µm. (C) CA4P induced contraction in endothelial cells and inhibited the formation of normal microtubule aggregates in HUVECs. After 18 h, microtubules (red) in HUVECs were

Combretastatin A-4 phosphate (CA4P) is a classical VDA that inhibits microtubule polymerization.[17,18] CA4P shows high selectivity for tumor vasculature by selectively blocking the signaling pathway of the endothelial cell-specific connexin VE-cadherin.[19] Compared to most drugs used in tumor chemotherapy, CA4P seldom causes any detectable lymphopenia or lymphoid cell depletion, nor does it inhibit the immune response.[20,21] Given the beneficial impacts of CA4P, it is promising to test whether this vascular-targeting small-molecule drug can enhance the therapeutic effect of CAR-T cells on solid tumors.

In the present study, we found that CA4P can effectively promote CAR-T cell infiltration in different *in vivo* solid tumor models and significantly improve the antitumor ability of CAR-T cells targeting different solid tumors. Our results indicate that combined treatment with CA4P and CAR-T cells is a promising strategy for treating different types of solid tumors.

RESULTS

CA4P Inhibits the Polymerization of Microtubules in Human Umbilical Vascular Endothelial Cells

It has been reported that CA4P inhibits tumor growth by selectively damaging tumor vessels,[22] resulting in a 100-fold decrease in tumor blood flow,[23] ischemia, and ultimately extensive tumor necrosis.[24] To evaluate the effect of CA4P on blood vessels *in vitro*, we first titrated CA4P to observe the dose-dependent effect on the proliferation of human umbilical vascular endothelial cells (HUVECs) and found that CA4P inhibited HUVEC proliferation at a concentration of 0.1 ng/mL or higher (Figure 1A, p < 0.01).

Endothelial cell motility plays an important role in supporting the survival of vascular endothelial cells and the pattern of neovascularization. As a typical antitubulin drug, CA4P can not only block the proliferation of endothelial cells but it also inhibits the movement of endothelial cells, resulting in weakening of tumor blood vessels.[19] To evaluate the effect of CA4P on endothelial cell motility, we analyzed the influence of CA4P on the migration of HUVECs. A wound-healing assay showed that compared with the untreated group, the group treated with 0.01 µg/mL CA4P exhibited inhibited migration (Figure 1B). To investigate the mechanism by which CA4P changes the morphology of vascular endothelial cells, we further examined the effect of CA4P treatment on normal microtubule aggregation and morphological changes in HUVECs. Using immunofluorescence analysis, we found that CA4P disrupted microtubule aggregation in HUVECs at a concentration of 0.001 ng/mL, and higher concentrations of CA4P treatment disturbed the polymerization of microtubules and caused morphological deformation in HUVECs (Figure 1C). These results suggest that CA4P suppresses the polymerization of microtubules in vascular endothelial cells and induces morphological deformation in endothelial cells, which may

---

stained with an anti-β-tubulin antibody (ab11307, Abcam) and analyzed by confocal fluorescence microscopy after incubation with CA4P (ng/mL) or PBS (control). Nuclei (blue) were stained with Hoechst 33342. Scale bars, 20 µm.

promote the destruction of the vascular network in solid tumors *in vivo*.

HER2-CAR-T Cells Combined with a Single CA4P Treatment Inhibit Tumor Growth in a SKOV3 Cell-Derived Xenograft Model

To explore the combined effect of CA4P and CAR-T cell therapy, we first generated CAR-T cells that specifically target HER2 (Figure S1A),[25] which is overexpressed in multiple types of solid tumors.[26] Approximately 44.52% of the T cells were HER2-CAR positive (Figure S1B). CD8+ T cells were dominant among the HER2-CAR-T cells (Figures S1C and S1D),and the proportion of central memory T cells (CD45RO+CCR7+CD62L+) was higher in the HER2-CAR-positive population than a control population (51.85% versus 41.14%, respectively) (Figures S1E and S1F), and expressed low levels of the exhaustion markers PD1 (27.52%), LAG3 (1.3%), Tim3 (0.27%), and TIGT (7.76%) (Figures S1G and S1H). The HER2-CAR-T cells also showed specific cytotoxicity against HER2-positive cancer cell lines, including the HCT116, SKOV3 and MDA-MB-231 cell lines, but had no obvious killing effect on HER2-negative tumor cells, such as Raji cells (Figures S2A and S2B). Compared with that of normal T (NT) cells, the cytotoxic effect of the HER2-CAR-T cells on HER2+ SKOV3 cells was enhanced with increasing effector-to-target (E:T) ratios, as was the secretion of IL2 and IFN-γ (Figure S2C). Next, we examined the effects of CA4P on the proliferation of cancer cells and HER2-CAR-T cells. The results showed that CA4P at a concentration of 0.1 ng/mL or higher could inhibit the proliferation of SKOV3 (ovarian cancer cell line) and HT-29 (colon cancer cell line) cells (Figures S3A and S3B, $p < 0.01$), and the inhibitory effect of CA4P on the proliferation of HER2-CAR-T cells began to appear at 10 ng/mL (Figure S3C, $p < 0.01$), suggesting that tumor cells are more sensitive to CA4P treatment than are CAR-T cells.

To evaluate the combined effect of CA4P and HER2-CAR-T cells *in vivo*, we first injected HER2-CAR-T cells into NOD-Prkdc scid IL-2rg null (NPG) mice that were transplanted with SKOV3 (HER2+) cancer cells, and untreated T cells were used as a control. For the group receiving the combined treatment with CA4P, CA4P was intraperitoneally injected into the mice before CAR-T cell infusion (Figure 2A). We next analyzed whether there was a synergistic effect of CA4P and HER2-CAR-T cells on the ability to kill SKOV3 cancer cells *in vivo*. More importantly, compared with the other groups, the group treated with HER2-CAR-T cells combined with CA4P showed a significantly better survival rate (Figure 2B). Tumor growth was inhibited by HER2-CAR-T cells alone compared with normal T cells or no treatment ($p < 0.001$). Importantly, the tumor volumes of the mice treated with HER2-CAR T cells in combination with CA4P were smaller than those of the mice treated with HER2-CAR-T cells alone ($p < 0.001$), suggesting that the inhibition of tumor growth by HER2-CAR-T cells was significantly enhanced by CA4P treatment (Figure 2C). In support of this result, we found rare Ki-67+ tumor cells in the group treated with HER2-CAR-T cells combined with CA4P compared with the group treated with HER2-CAR-T cells alone (Figure 2D). Further analysis showed that more

necrosis occurred within the tumor tissue in the group treated with HER2-CAR-T cells combined with CA4P compared with the group treated with HER2-CAR-T cells alone (Figure 2D). In addition, apoptosis was induced in a significant portion of tumor cells in the group treated with HER2-CAR-T cells combined with CA4P, whereas less apoptosis in tumor cells was observed in the group treated with HER2-CAR-T cells alone (Figure 2E). In addition, the weight of the mice in the combination group did not change significantly (Figure 2F), and no obvious depilation, rashes or mental burnout were observed, which suggested no serious side effects occurred in the combined treatment group.

Collectively, these results suggest that compared with treatment with HER2-CAR-T cells alone, treatment with HER2-CAR-T cells combined with CA4P has an enhanced ability to suppress the growth of SKOV3 tumor cells in a cell-derived xenograft (CDX) model.

HER2-CAR-T Cells Combined with Multiple CA4P Treatments Eliminate Large Solid Tumors in the SKOV3 CDX Model

We next tested whether CA4P treatment combined with HER2-CAR-T cells can reduce a large tumor burden, which is a challenge in solid tumor therapy. To this end, we used SKOV3 cell-transplanted NPG mice with tumor sizes larger than 150 mm³. To enhance the effect of CA4P treatment, we applied a protocol of multiple CA4P treatments. CA4P intraperitoneal injection was first performed before the infusion of CAR-T or GFP-T cells. Subsequent CA4P treatments were given twice a week for a total of five times (Figure 3A). Compared with no treatment, CA4P treatment alone could inhibit the growth of tumors to some extent, but it did not achieve statistical significance (n = 6, p = 0.4566). However, compared with other treatments, the treatment of HER2-CAR-T cells combined with multiple CA4P treatments significantly reduced the volume of tumors *in vivo* ($p < 0.01$) (Figure 3B). Importantly, two out of the six mice in this group showed complete tumor elimination (Figure S3D). Furthermore, the group treated with HER2-CAR-T cells combined with multiple CA4P injections displayed a longer survival period than did the other groups, suggesting synergy between the CAR-T cells and CA4P treatment (Figure 3C). Immunostaining for the HER2 antigen showed that HER2+ tumor cell numbers were significantly reduced in the group treated with HER2-CAR-T cells combined with multiple CA4P injections compared with the other groups (Figure 3D).

Taken together, these results suggested that multiple CA4P treatments in combination with CAR-T cell therapy could reduce large tumor burdens in CDX mouse models.

CA4P Assists CAR-T Cell Infiltration into Tumor Tissue and Increases IFN-γ Secretion

To explore how CA4P promotes the therapeutic effect of CAR-T cells on solid tumors, we first analyzed CAR-T/T cell retention and infiltration in xenograft tumors in mice after CA4P treatment. We used immunohistochemistry to assess the infiltration of T cells (CD3) into the tumors of mice in each group. CD3+ T cells were found in the groups treated with HER2-CAR-T cells alone and HER2-CAR-T
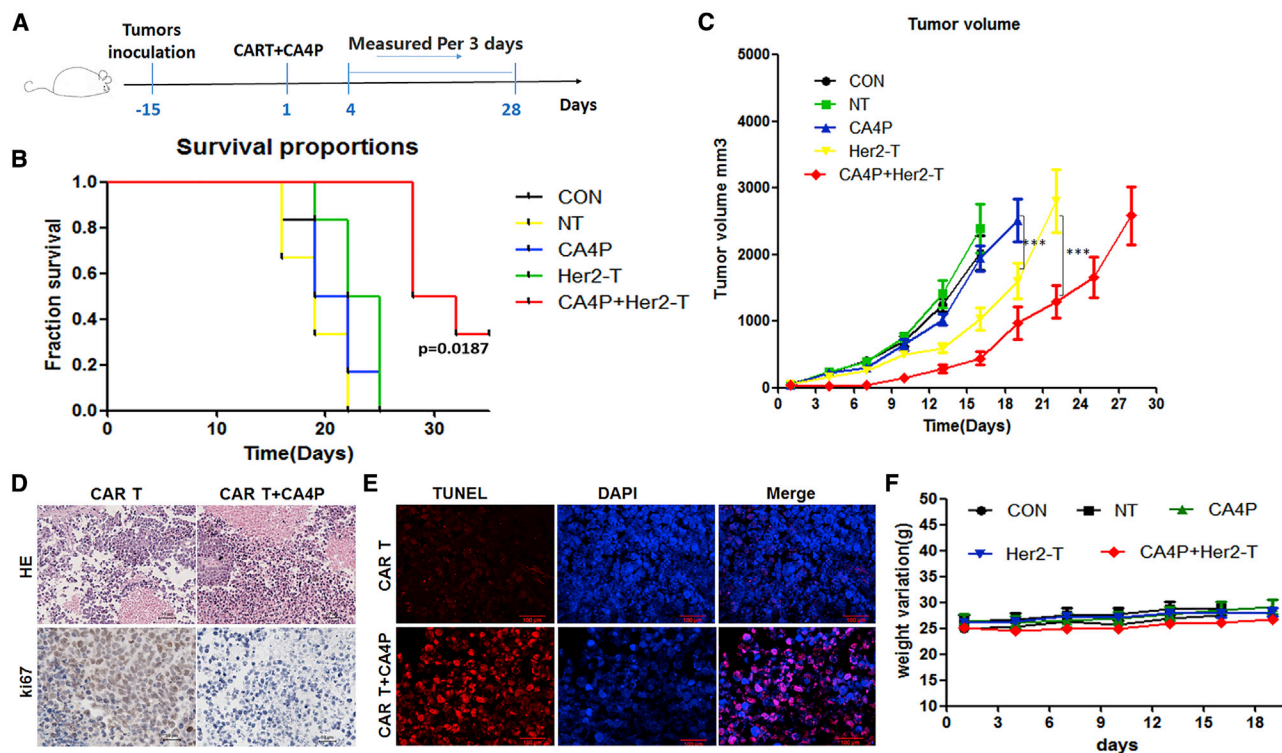
Figure 2. SKOV3 Cell-Derived Xenograft Model Treated with HER2-CAR-T Cells in Combination with a Single CA4P Treatment

(A) Diagram of the CAR-T cells accompanied by CA4P *in vivo* experiment. The SKOV3 cell-derived xenograft (CDX) model was established in NPG mice with 1×10^6 SKOV3 cells by subcutaneous injection. Approximately 2 weeks after tumor cell injection, normal T (NT) or HER2 CAR-T cells were injected into mice via the tail vein at a dose of 5×10^6 cells per mouse. For the group treated with the combined therapy, CA4P was intraperitoneally injected into the mice at a dose of 100 mg/kg 4–6 h before NT/CAR-T cell infusion. (B) Kaplan-Meier survival analysis of all groups. The group treated with HER2-CAR-T cells combined with CA4P had a longer survival time than did the other groups. (n = 6). (C) Tumor growth curves of different groups. The tumor volumes of the mice in different groups, including the NT group, CON (untreated) group, CA4P (CA4P alone) group, HER2-T (HER2-CAR-T cells alone) group, and CA4P+HER2-T (HER2-CAR-T cells combined with CA4P) group, were compared (volume calculation: long diameter × wide diameter × wide diameter/2, n = 6, p < 0.001). (D) H&E staining and immunohistochemical analysis of Ki-67 expression in mouse tumor tissue samples from the HER2-CAR-T cell group and the HER2-CAR-T cells combined with CA4P group. (E) Analysis of TUNEL staining used to evaluate the degree of apoptosis in the HER2-CAR-T cell group and the HER2-CAR-T cells combined with CA4P group. Red fluorescence shows apoptotic cells; blue DAPI fluorescence indicates nuclei. Scale bars, 100 μm. (F) The weights of the mice in all groups (n = 6).

cells combined with CA4P treatment, suggesting T cell infiltration occurred in these two groups (Figure 4A). More importantly, the combined treatment group had a higher proportion of CAR-T cells in the peripheral blood at 22 days (p = 0.0119) and 29 days (p = 0.0173) post-treatment than did the HER2 CAR-T cells alone group (Figure 4B), and the proportion of T cells in the tumor tissue in the combined treatment group was higher than that in the HER2-CAR-T cells alone group (p < 0.01) (Figure 4C), suggesting that CA4P treatment specifically promotes the infiltration of HER2-CAR-T cells into the tumor site. In support of these results, the expression of the blood vessel marker CD31 was significantly downregulated in the groups treated with CA4P, suggesting that CA4P treatment could impair the blood vessels in the tumor site (Figures 3D and 3E) *in vivo*. As a control, there was no significant difference in the proportion of splenic T cells between these two groups (p = 0.3434) (Figure 4D). Collectively, these results suggested that CA4P-assisted HER2-CAR-T cells had higher capacities of *in vivo* expansion and tumor infiltration than did unassisted HER2-CAR T cells.

Next, we analyzed the expression of several T cell-associated cytokines and molecules, including interferon (IFN)-γ, tumor necrosis factor alpha (TNFα), interleukin (IL)-12, granzyme B, vascular endothelial growth factor (VEGF), IL-4, and IL-2, in peripheral blood samples from all groups 1 month after the first treatment. Notably, IFN-γ expression increased significantly in the HER2-CAR-T group and HER2-CAR-T combined with CA4P group compared with the other groups (p < 0.01) (Figure 4E), which was consistent with the result for IFN-γ secretion in an *in vitro* test validating HER2-CAR-T cell functions (Figure S2C). Moreover, the expression of IFN-γ in the HER2-CAR-T combined with CA4P group was significantly higher than that in the CAR-T cells alone group (p < 0.01) (Figure 4E). Consistent with these results, the levels of CD3$^+$ T cells (CD3E, p = 0.015; CD3D, p = 0.026) and IFN-γ (p = 0.14) could be potential markers for prognosis prediction, as revealed by Kaplan-Meier survival analysis (Figures 4F and 4G; TIMER database: https://cistrome.shinyapps.io/time).[27] Accordingly, in addition to increasing the infiltration of CAR-T cells in
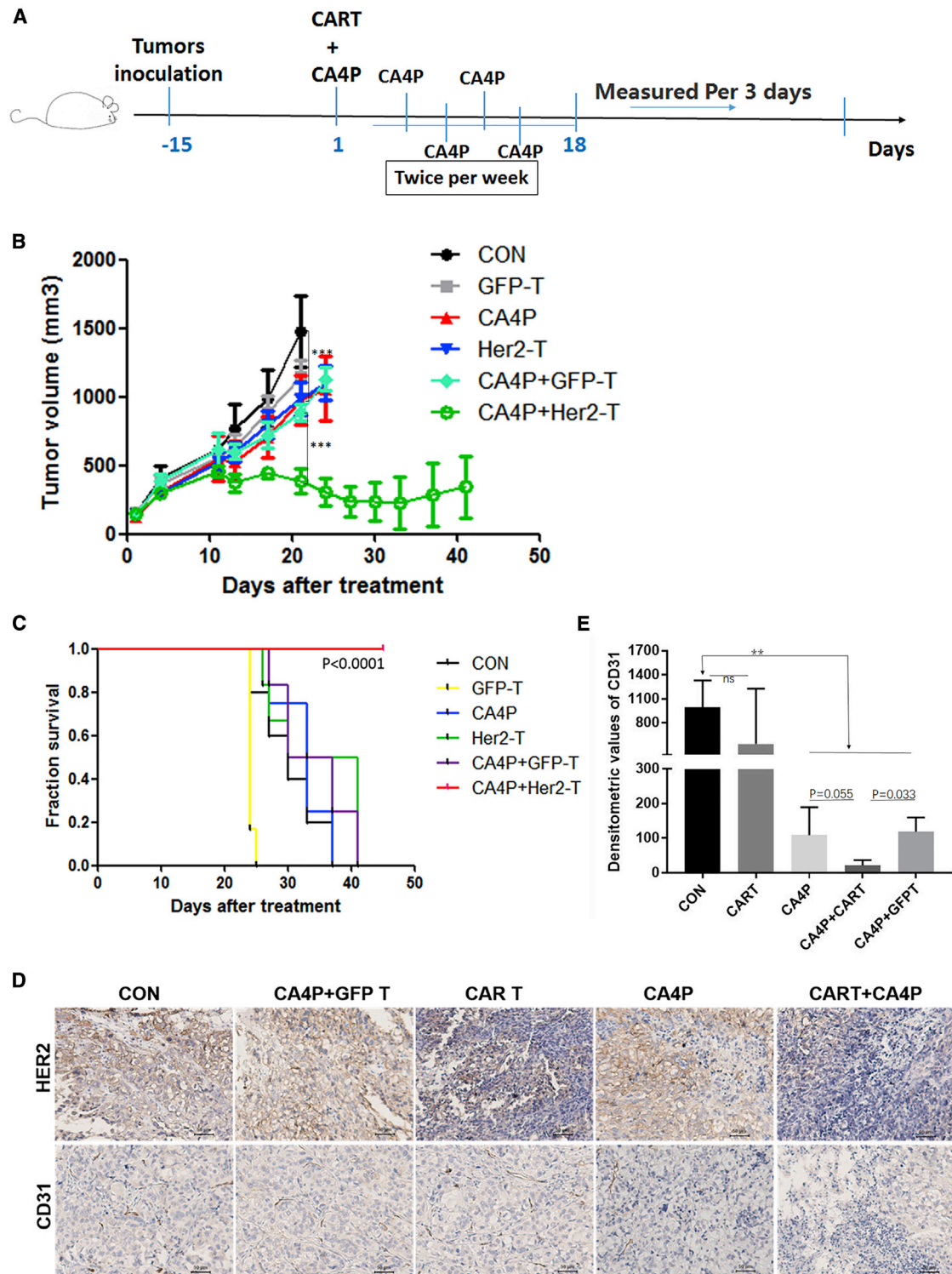
Figure 3. SKOV3 CDX Model Treated with HER2-CAR-T Cells in Combination with Multiple CA4P Treatments

(A) Diagram of the CAR-T cells accompanied by CA4P *in vivo* experiment. The SKOV3 CDX model was established in NPG mice with 2×10^6 cells by subcutaneous injection. The treatments were carried out when the tumor size was approximately 150 mm³. The mice were randomly divided into five groups. HER2-CAR-T cells (2.5×10^6) were infused into the CDX model mice via the tail vein, as were GFP-T cells. For the combined therapy group, CA4P was intraperitoneally injected into the mice at a dose of

(legend continued on next page)

tumor sites, CA4P treatment may also enhance the secretion of IFN-γ by CAR-T cells *in vivo*.

HER2-CAR-T Cells Combined with CA4P Treatment Inhibit Tumor Growth in Patient-Derived Xenotransplantation Mouse Models of Colorectal Cancer

A tumor cell line is different from tissue samples from tumor patients. To explore the therapeutic effect of the combined therapy on patient-derived tumors, we chose HER2-positive colorectal cancer and a patient-derived xenotransplantation (PDX) model, which more closely matches patient characteristics, to test the combined CA4P therapy strategy. Referring to our previous experimental protocols, we established a PDX model with tumor tissue derived from a colorectal cancer patient.[28] HER2-CAR-T cell (or GFP-T cell) infusions with or without CA4P treatments were carried out when the average tumor volume was approximately 150 mm^3 in NPG mice. The cell infusions were intravenously injected via the tail vein at a dose of 1×10^6 cells per mouse. The mice were divided into the following groups: GFP-T cells alone, HER2-CAR-T cells alone, CA4P treatment alone, GFP-T cells combined with CA4P treatment, and HER2-CAR-T cells combined with CA4P treatment. CA4P was intraperitoneally injected into each mouse at a dose of 100 mg/kg 4–6 h before the infusion of GFP-T/CAR-T cells. The treatments including cell infusion and CA4P injection were conducted three times at intervals of every other week (Figure 5A). Compared with the CA4P alone, GFP-T cell treatment alone, and HER2-CAR-T cell treatment alone groups, the HER2-CAR-T cells combined with CA4P treatment group exhibited an inhibition of tumor growth, as determined by evaluating tumor volume (p < 0.01) (Figure 5B). Compared with those in the other groups, the NPG mice in the combined treatment group did not show a significant decrease in weight (Figure 5C), and no obvious depilation, rashes, or mental burnout were observed, which suggested that no serious side effects occurred in the combined treatment group.

Necrosis in tumor tissue was detected with H&E staining. The results showed that the CAR-T cells combined with CA4P treatment group exhibited more necrosis than did the other groups (Figure 5F), suggesting a stronger antitumor effect for the combined treatment. The HER2 antigen was detected by immunohistochemistry in each group after treatment. The results showed that HER2 antigen expression decreased in the HER2-CAR-T cell treatment alone group. Weaker HER2 antigen expression was displayed in the combined treatment group, suggesting that most HER2-positive cells were killed in the combined treatment group (Figure 5F).

The infiltration of T cells was detected with an anti-CD3 antibody by immunohistochemistry. There were more T cells in the tumor tissue in the group treated with CA4P combined with CAR-T cells (Figure 5F). Peripheral blood samples from the mice were dynamically monitored by flow cytometry. The results showed that there was a higher proportion of CAR-T cells in the combined treatment group than in the HER2-CAR-T cell treatment alone group at 28 and 42 days after the first treatment (Figure 5D, p < 0.01). More detailed data for the detection of CAR-T cells in the peripheral blood of the combination group mice are displayed in Figure 5E.
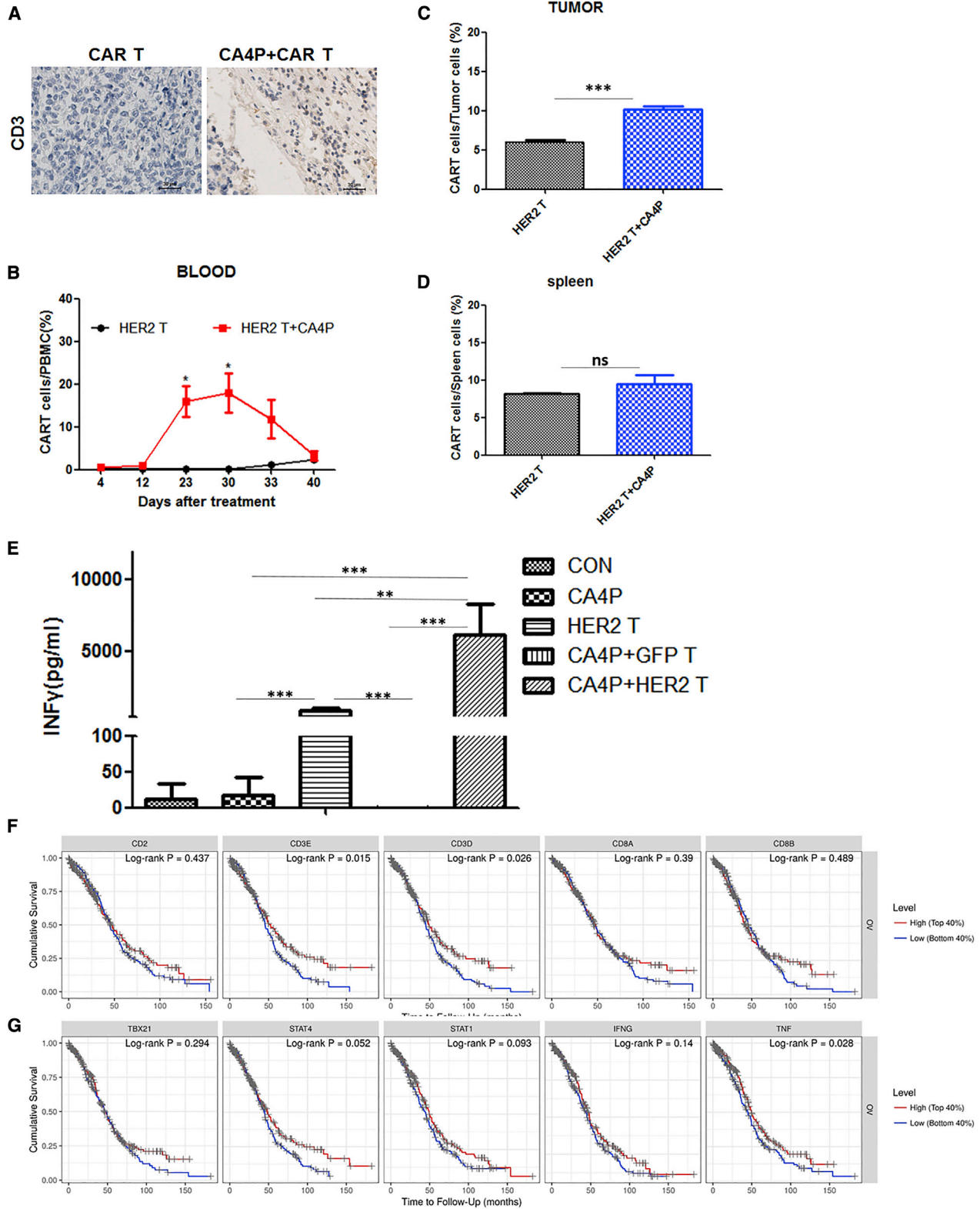
CD31 expression in tumor tissue was analyzed by immunohistochemistry in the untreated, CA4P alone, HER2-CAR-T cells alone, and HER2-CAR-T cells combined with CA4P treatment groups. Weaker expression of CD31 was shown in the group treated with HER2-CAR-T cells alone than in the untreated group and the CA4P alone group. Compared with the HER2-CAR-T cells alone group, the combined treatment groups displayed lower expression of CD31, suggesting more extensive destruction of tumor vessels (Figure S4B). In addition, the immunohistochemical analysis also indicated upregulated expression of PD-L1 in the HER2-CAR-T cells alone and CAR-T cells combined with CA4P treatment groups (Figure S4B). IFN-γ from CD8$^+$ lymphocytes upregulates PD-L1 expression in ovarian cancer cells and restrains tumor growth. Lymphocyte infiltration and IFN-γ secretion may be the keys for the treatment of ovarian cancer using anti-PD-1 therapy.[29,30] Consistent with our study, *in vitro* experiments showed that IFN-γ could increase the expression of PD-L1 in an ovarian cancer cell line in a dose-dependent manner (Figure S4A).

These results suggested that CA4P-assisted HER2-CAR-T cell therapy has a better antitumor effect than do other treatments on the colorectal cancer PDX model. The effects of the combined treatment involve the destruction of tumor vessels, promotion of T cell infiltration, proliferation of CAR-T cells, and decreased expression of the HER2 antigen.

Mesothelin-CAR-T Cells Combined with CA4P Inhibit Tumor Growth in PDX Mouse Models of Ovarian Cancer

Are the effective antitumor effects of therapy with CA4P and CAR-T cells limited to HER2-CAR-T cells? Can this strategy be used to target other antigens or with other CAR-T cells? To address these issues, we chose another tumor antigen, mesothelin (Meso), to test the combination strategy. Meso is a specific surface protein on ovarian cancer

---

100 mg/kg 4–6 h before GFP-T/CAR-T cell infusion, and subsequent CA4P treatments were administered twice a week for a total of five times. (B) Tumor growth curves of different groups. Compared with CA4P treatment alone, GFP-T cell treatment, and no treatment, treatment with HER2-CAR-T cells alone could significantly inhibit the growth of tumors (n = 6, p < 0.01). Compared with no treatment, CA4P treatment alone could inhibit the growth of tumors to some extent, but this difference was not statistically significant (n = 6, p = 0.4566). (C) Kaplan-Meier survival analysis of all groups. The HER-CAR-T cells combined with CA4P group displayed a longer survival time than did the other groups (n = 6). (D) The effect of the combination therapy on blood vessels and HER2 expression was examined *in vivo*. Immunohistochemical analysis of tumor tissue samples showed that CD31 and HER2 expression was different among the untreated group, the HER2-CAR-T cells alone group, and the CAR-T cells combined with CA4P treatment group. Scale bars, 50 μm. (E) Optical densitometric statistical analysis of the individual bands in (D) was performed using GraphPad Prism5 software between the groups. Optical densitometric calculation of five randomly selected visual fields in each group was performed using ImageJ software. Optical densitometric = Positive area × Average densitometric value.

A

CAR T · CA4P+CAR T

CD3

B

BLOOD

C

TUMOR

D

spleen

E

CON
CA4P
HER2 T
CA4P+GFP T
CA4P+HER2 T

F

CD2 · CD3E · CD3D · CD8A · CD8B

Log-rank P = 0.437 · Log-rank P = 0.015 · Log-rank P = 0.026 · Log-rank P = 0.39 · Log-rank P = 0.489

G

TBX21 · STAT4 · STAT1 · IFNG · TNF

Log-rank P = 0.294 · Log-rank P = 0.052 · Log-rank P = 0.093 · Log-rank P = 0.14 · Log-rank P = 0.028

Time to Follow-Up (months)

(legend on next page)

tumors. We established a PDX model of ovarian cancer in NPG mice. Using the same design and preparation process as those used for the HER2-CAR-T cells (Figure S5A), Meso-CAR-T cells were prepared from healthy donor peripheral blood mononuclear cells (PBMCs). The proportion of Meso-CAR-T cells was up to 54.3% (Figure S5B) and a high CD8$^+$/CD4$^+$ ratio (Figures S5C and S5D). The phenotypes of the Meso-CAR-T cells were mainly naive and central memory, which is similar to the phenotypes that have been detected as HER2-CAR-T cells above (Figures S5E and S5F).[31] The CAR-T cells also exhibited low expression levels of exhaustion markers (Figures S5G and S5H).

A standard luciferase-based bioluminescence assay was used to evaluate the cytotoxicity of the Meso-CAR-T cells. The results suggested that the Meso-CAR-T cells had a specific cytotoxic effect on cells expressing the Meso antigen and no cytotoxic effect on Meso$^-$ cells (Figures S5I and S5J). We adapted protocols similar to those used for the colorectal PDX model to establish a Meso$^+$ ovarian cancer PDX model[28] treated with Meso-CAR-T cell therapy. CAR-T cell infusions or CA4P treatments were carried out when the average tumor volume was approximately 150 mm^3 in the NPG mice. Each mouse was intravenously infused with 1×10^6 cells via the tail vein. CA4P was intraperitoneally injected into each mouse at a dose of 100 mg/kg 4–6 h before the infusion of the CAR-T cells. The treatments including cell infusion and CA4P injection were conducted every other week, and three total treatments were administered (Figure 6A).

Compared with the group treated with Meso-CAR-T cells alone, the group treated with Meso-CAR-T cells combined with CA4P exhibited an inhibition of tumor growth based on tumor volume measurements (p < 0.01) (Figure 6B). The mice that received Meso-CAR-T cells combined with CA4P had a longer survival period than did the mice treated with Meso-CAR-T cells alone (Figure 6C). IFN-γ in the peripheral blood showed higher levels in the combined treatment group than in the other group (Figure 6D). The weight of the NPG mice in both groups did not decrease significantly (data not shown), and no obvious depilation, rashes, or mental burnout were observed, which suggested that no serious side effects occurred in the combined treatment group.

More extensive necrosis could be found in the Meso-CAR-T cells combined with CA4P treatment group than in the other group by

H&E staining. Terminal deoxynucleotidyltransferase-mediated deoxyuridine triphosphate nick end labeling (TUNEL) staining showed more tumor cell apoptosis in the combined treatment group than in the other groups (Figures 6E and 6F). Additionally, there was more T cell infiltration and less CD31 and Meso expression detected by immunohistochemical analysis in the combined treatment group than in the other treatment group (Figure 6E).

These results suggest that CA4P-assisted Meso-CAR-T cell therapy has more effective antitumor activities than do other treatments in the ovarian cancer PDX model. The activities of the treatment with CAR-T cells combined with CA4P may involve the destruction of tumor vessels, promotion of T cell infiltration, proliferation of CAR-T cells, and increased expression of secreted IFN-γ.

DISCUSSION

The combination of CAR-T cells and CA4P showed effective antitumor activities in colon (HER2$^+$) and ovarian (Meso$^+$) tumor models. The overall survival rate of mice receiving the combined treatment was higher than that of mice receiving any single treatment. The combined group exhibited less tumor-related antigen expression and more tumor tissue necrosis and tumor cell apoptosis than did the other groups. In addition, CA4P promoted T cell infiltration and enhanced IFN-γ secretion in both the CDX and PDX mouse models.

CAR-T cells recognize surface antigens of tumor cells and exhibit specific cytotoxicity against these malignant cells. The expansion and persistence of adoptively transferred T cells is necessary for a sustained antitumor effect.[32] In addition, even when a target antigen of a solid tumor is identified, a CAR-T cell must infiltrate the tumor site to kill tumor cells.[33] Only a minority of solid tumor types are reported to be effectively treated by CAR-T cells, and these types include glioblastoma, pancreatic cancer, mesothelioma, and sarcoma[34–42] to some extent. Until now, studies of CAR-T cell therapy alone have achieved limited progress in solid tumors.

The abnormal vascular and interstitial barrier is regarded as a key obstacle preventing CAR-T cells from infiltrating into tumor tissue and reacting to solid tumor cells. This abnormal neovascular structure in tumors helps to establish the tumor microenvironment and maintains drug resistance, such as immunosuppression and chemotherapeutic resistance.[43] Therefore, the destruction or inhibition of the neovascular system is a key step before CAR-T cell treatment. Via

Figure 4. Detection of the T Cell Proportion, IFN-γ Secretion within the Peripheral Blood Cell Population, and T Cell Infiltration into Tumor Tissue in the SKOV3 CDX Model Treated with HER2-CAR-T Cells in Combination with Multiple CA4P Treatments

(A) Immunohistochemical detection of the infiltration of T cells (CD3) in the HER2-CAR-T cell group and in the HER2-CAR-T cells combined with CA4P group. Scale bars, 30 μm. (B) Comparison of peripheral blood of mice in the HER2-CAR-T cells alone group and the HER2-CAR-T cells combined with CA4P group by flow cytometry. The combined CA4P group had a higher proportion of CAR-T cells after 22 days (n = 3, p = 0.0119) and 29 days (n = 3, p = 0.0173) of treatment. (C) The proportion of T cells in tumors from the combined treatment group was higher than that in the tumors from the HER2-CAR-T cells alone group (n = 3, < 0.01)). (D) There was no significant difference in the proportion of splenic T cells between the two groups (n = 3, p = 0.3434). (E) ELISA detection of the IFN-γ level in the peripheral blood of mice in each treatment group 1 month after treatment (n = 3, p < 0.001). (F) Comparison of the Kaplan-Meier survival curves classified by CD3 and CD8 expression in different types of cancer. The results showed that the CD8/CD3 ratio was positively correlated with prognosis in ovarian cancer (CD3E, p = 0.015; CD3D, p = 0.026; and CD8a, p = 0.39) (TIMER database: https://cistrome.shinyapps.io/time). (G) Positive correlations of the T helper 1 (TH1) cell quantity and TNF expression with prognosis by Kaplan-Meier survival analysis. TNF (p = 0.028) and IFN-γ (p = 0.14) (the TIMER database).
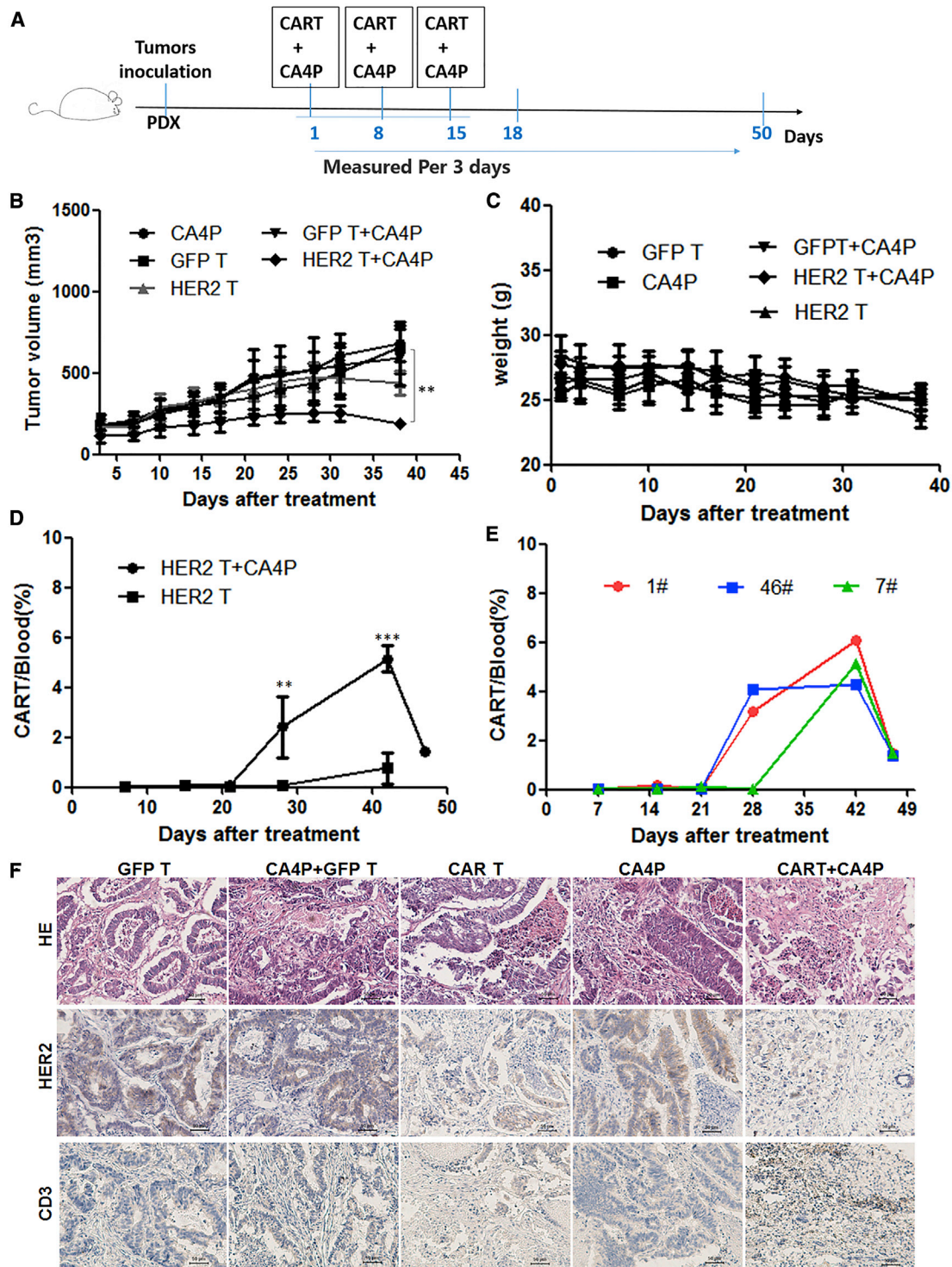
Figure 5. PDX Mouse Models of HER2-Positive Colorectal Cancer Treated with HER2-CAR-T Cells Combined with CA4P

(A) PDX models were established using tissue derived from a HER2-positive colorectal patient. Further cell infusions or CA4P treatments were carried out when the average tumor volume was approximately 150 mm³ in NPG mice. Cells were intravenously infused via the tail vein at a dose of 1×10^6 cells per mouse. The mice were divided into the following treatment groups: normal T (NT) cells, HER2-CAR-T cells, NT cells combined with CA4P treatment, and HER2-CAR-T cells combined with CA4P treatment. CA4P was injected into each mouse intraperitoneally at a dose of 100 mg/kg 4–6 h before the infusion of NT/CAR-T cells. The treatments including cell infusion and CA4P injection

(legend continued on next page)

binding to the colchicine binding site on tubulin, CA4P inhibits microtubule polymerization.[17,18] In addition, CA4P shows high selectivity for tumor vasculature due to selective blocking of the signaling pathway of the endothelial cell-specific connexin VE-cadherin.[19] Therefore, CA4P restrains tumor growth by selectively damaging tumor vasculature, which reduces tumor blood flow and leads to extensive tumor necrosis.[22–24,44,45] In our study, CA4P inhibited the proliferation and migration of HUVECs, disrupted the polymerization of microtubules, and caused morphological deformation in HUVECs *in vitro*, and CA4P treatment could impair blood vessels in the tumor site *in vivo*. These effects would increase vascular permeability and promote the infiltration of CAR-T cells into solid tumors. To enhance the auxiliary effect, CAR-T cells were infused into mice 4–6 h after the injection of CA4P in this study. This design helped CAR-T/T cells traffic to the inner regions of solid tumors. Currently, there are no similar results in the treatment of solid tumors with vascular interference agents other than CA4P combined with CART, which is worthy of our further study.

Sengupta et al.[46] showed that CA4P combined with doxorubicin treatment increases the therapeutic index and alleviates side effects. Clinical trials studying the treatment of cancer patients suggest that combination with CA4P improves the therapeutic outcomes of patients treated with carboplatin and paclitaxel.[47] In our study, CA4P injection in combination with CAR-T cell infusion displayed synergistic antitumor effects on colorectal and ovarian tumor models. With this combination therapy, the infiltration of T cells was shown in tumor tissues, while the peripheral blood showed the accumulation of CAR-T cells as well as an enhanced IFN-γ level in the CDX and PDX mouse models. Specific to function, IFN-γ secreted by CD8+ CAR-T/T cells is also involved in decreases in VEGF secretion and angiogenesis.[48] Moreover, IFN-γ directly induces tumor angiogenesis degeneration in endothelial cells.[49] The reason for the high level of IFN-γ secretion is that CAR-T cells specifically recognize a surface antigen on tumors and secrete cytokines to enhance cytotoxicity to malignant cells.

It is necessary to adopt various approaches to overcome the potential limitations of CAR-T cells in the treatment of solid tumors. The more effective combined treatment will be considered for cancer immunotherapy. The key point to make is that this combination has synergistic effects on tumor cells and their microenvironment. CA4P therapy disrupts the tumor neovascular system and causes necrosis in tumors, which is correlated with T cell or drug infiltration into tumors. Full exposure of CAR-T cells to tumor antigens results in the secretion of high levels of cytokines (such as IFN-γ) and cytotoxicity to intratumor cells. Then, IFN-γ more extensively inhibits tumor angiogenesis. CA4P and CAR-T cells exerted synergistic effects on colorectal and ovarian tumor models in our study. Even so, the toxicity of the combined application of CAR-T cells and CA4P needs to be further evaluated in clinical trials. Consistent with our results, some evidence also showed that the IFN-γ secreted by the infiltrated CD8+ T cells could upregulate PD-L1 expression in ovarian cancer cells and restrain tumor growth.[29,30] We can imagine our CA4P plus CAR-T cell strategy combined with immune checkpoint blockade, such as anti-PD-L1 or anti-PD-1 therapy,[29,30] to obtain better antitumor effects.

MATERIALS AND METHODS

Cell Lines and Culture
The HCT116, SKOV3, MDA-MB-231, PANC1, A549, and Raji cell lines obtained from the National Infrastructure of Cell Line Resource (Beijing, China), and human HEK293T cells (ATCC, USA), were all cultured in DMEM (Gibco, USA), except for the Raji cells, which were cultivated in RPMI 1640 medium (Gibco, USA). Both media were supplemented with 10% heat-inactivated fetal bovine serum (FBS; Gibco, USA), and the cells were incubated in a humidified incubator with 5% CO_2 at 37°C and passaged every 2 days with a complete culture medium change.

Plasmid Construction and Lentivirus Production
A DNA sequence encoding a single-chain variable fragment (scFv), CD8α hinge and transmembrane region, a 4-1BB costimulatory signaling domain, and the cytoplasmic region of the CD3ζ chain was synthesized by BGI Genomics (Beijing, China). The CAR encoded by the DNA sequence was inserted into a self-inactivating (SIN) pRRL lentiviral vector with XbaI and SalI sites. The lentiviral vector (16 μg), psPAX2 (12 μg), and pMD2.G (4 μg) were cotransfected into HEK293T cells in 10-cm dishes with the calcium phosphate method as previously described.[25] The medium was changed after 12 h. The supernatants were collected after a subsequent 24–48 h of cultivation. These supernatants were filtered through 0.22-μm polyvinylidene fluoride filters (Millipore, USA) and stored at −80°C for future use.

Generation of CAR-T Cells
All PBMCs used in our study were obtained from healthy donors. CD3+ T cells were cultured in X-VIVO 15 medium (Lonza) supplemented with 10% FBS and 100 U/mL IL-2 (PeproTech, USA). These cells were prestimulated with anti-CD3/CD28 beads (Thermo Fisher

were conducted every other week, and three total treatments were administered. (B) Tumor growth curves of different groups were created. Compared with the CA4P alone, NT treatment, and HER2-CAR-T cell treatment alone groups, the HER2-CAR-T cells combined with CA4P treatment group exhibited inhibited tumor growth, as determined by measuring tumor volume (n = 3, p < 0.01). (C) The weight of the mice in the combined treatment group did not change significantly (n = 3). (D) The peripheral blood in the mice was dynamically monitored by flow cytometry. The results showed that there was a higher proportion of CAR-T cells in the combined treatment group than in the CAR-T cells alone group at 28 and 42 days after the first treatment (n = 3, p < 0.01). More detailed data for CAR-T cell detection in the peripheral blood of the combined treatment group (1#, 46#, 7#) are displayed in (E). (F) CA4P and CAR-T cell-treated HER2-positive colorectal tumors were histopathologically analyzed. H&E staining and immunohistochemical analysis of tumor tissue samples showed that CD3 and HER2 expression differed among the untreated group, the HER2-CAR-T cells alone group, and the CAR-T cells combined with CA4P treatment group. Scale bars, 50 μm.
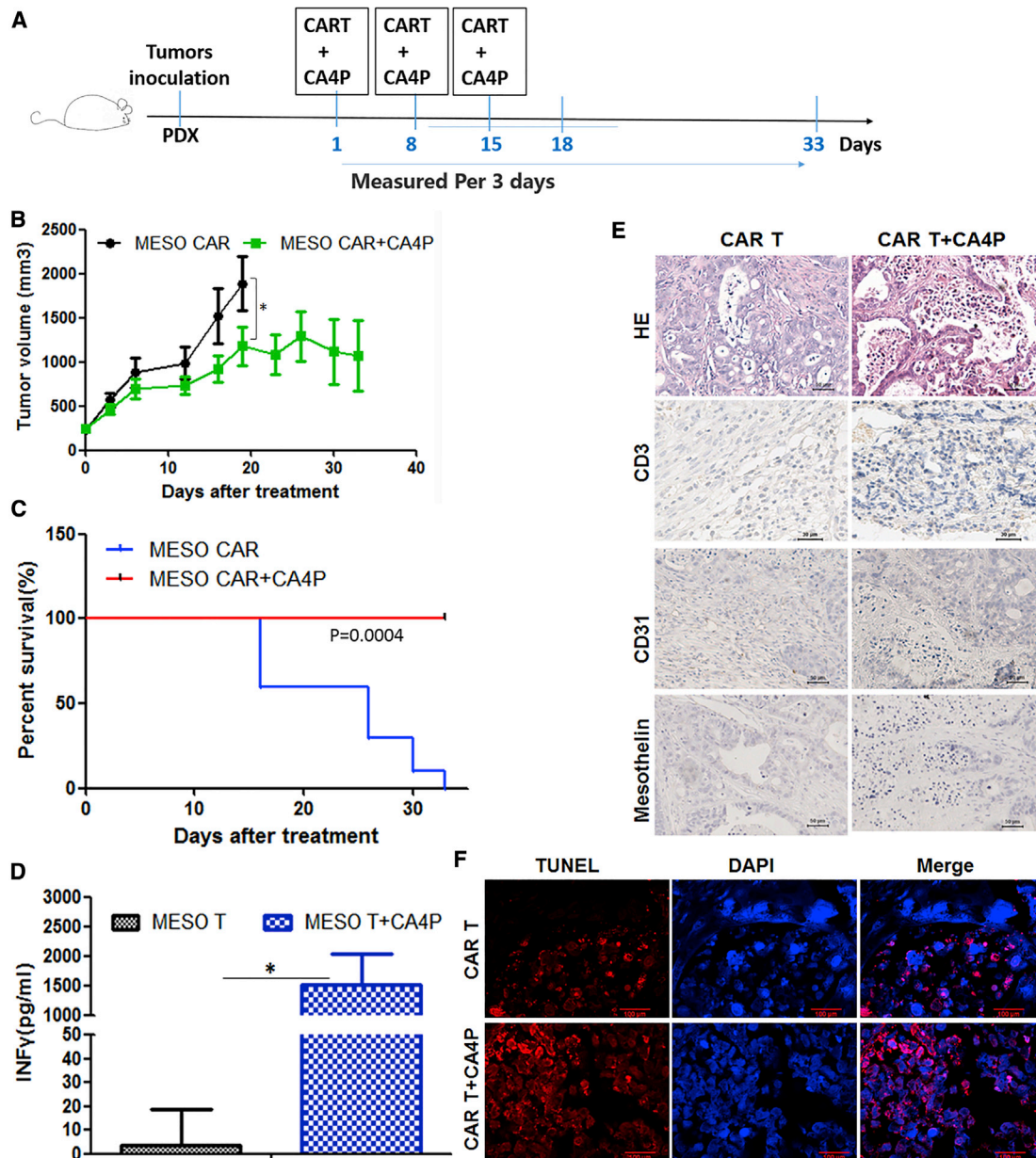
Figure 6. PDX Mouse Models of Meso[+] Ovarian Cancer Treated with Meso-CAR-T Cells Combined with CA4P

(A) PDX models were established using tissue derived from a Meso[+] ovarian cancer patient. Further cell infusions or CA4P treatments were carried out when the average tumor volume was approximately 150 mm³ in NPG mice. Cells were intravenously infused via the tail vein at a dose of 1×10^6 cells per mouse. The mice were divided into two groups: the Meso-CAR-T cell group and the Meso-CAR-T cells combined with CA4P treatment group. CA4P was injected into each mouse intraperitoneally at a dose of 100 mg/kg 4–6 h before the infusion of CAR-T cells. The treatments including cell infusion and CA4P injection were conducted every other week, and three total treatments were administered. (B) Tumor growth curves for the two groups are shown. The CAR-T cells combined with CA4P treatment group exhibited more inhibition of tumor growth than did the CAR-T cells alone group (n = 5, p < 0.05)). (C) Kaplan-Meier survival analysis of all groups is shown. The Meso-CAR-T cells combined with CA4P group displayed a longer survival time than did the CAR-T cells alone group. (D) The IFN-γ level in the peripheral blood of the mice in the two groups was detected by ELISA 20 days after treatment (n = 3, p < 0.05)). (E) Histopathological analysis was used to assess CA4P and CAR-T cell-treated Meso[+] ovarian tumors. H&E staining and immunohistochemical analysis of tumor tissue samples assessed the CD3, CD31, and Meso expression in these two groups, and more extensive necrosis and T cell infiltration and less CD31 and Meso expression was detected in the combined treatment group by immunohistochemical analysis. Scale bars, 50 μm. (F) Analysis by TUNEL staining was used to evaluate the degree of apoptosis. Red fluorescence shows apoptotic cells; blue DAPI fluorescence indicates nuclei. Scale bars, 100 μm. TUNEL analysis suggested more tumor cell apoptosis occurred in the combined treatment group than in the CAR-T cells alone group.

Scientific, USA) (1:1 bead-to-cell ratio) for 48 h and transduced with the CAR lentiviral vector. Transduction efficiency was evaluated by flow cytometry 6 days later.

Flow Cytometry

The expression and phenotype of CAR-T cells was examined by flow cytometry with an Alexa Fluor 647-conjugated anti-mouse/human IgG, F(ab′)₂ antibody (BioLegend). The fluorochrome-conjugated antibodies included anti-CD3, anti-CD4, anti-CD8, anti-CD45RO, anti-CD62L, anti-CD45RA, anti-LAG-3, anti-TIGT, anti-TIM-3, and anti-PD-1 (CD279) antibodies (all antibodies were purchased from BD Biosciences, USA). Isotype-matched fluorochrome-conjugated immunoglobulin (Ig) antibodies were used as negative controls. Flow cytometry was performed with a FACSCalibur and analyzed with its software (BD Biosciences, USA) or FlowJo 7.6.1.

Cytotoxicity Assay

To identify the cytotoxicity of CAR-T cells *in vitro*, a lentiviral expression vector for high antigen expression was constructed, and then target cells were transfected. The endogenous expression or overexpression of the corresponding antigen was confirmed by flow cytometry. Normal T or CAR-T cells and HER2/Meso⁺ or HER2/Meso⁻ tumor cells were cocultured in a 96-well plate for 20 h at a defined effector to target (E:T) ratio, and then cytotoxicity was evaluated by a standard bioluminescence assay based on luciferase.[25]

Cytokine Release Assay

Cytokine release was detected by an ELISA after 24 h of culture in the presence of normal T or CAR-T cells. Tumor cells that were HER2/Meso positive or HER2/Meso negative were cultivated in a 96-well plate. Normal T or CAR-T cells were cocultured with the tumor cells for 24 h at different E:T ratios. Briefly, the CAR-T cells were cocultured with the tumor cells (1×10^4) in RPMI 1640 medium at a final volume of 200 μL in 96-well plates. The supernatants were harvested after 24 h of coculture, and IFN-γ and IL-2 levels were measured with ELISA kits (BioLegend, San Diego, USA).

Cell Proliferation Assay

The effect of CA4P on cell proliferation was detected by a cell counting kit-8 (CCK8) assay. HT29 cells, SKOV3 cells, HER2-CAR-T cells, and HUVECs were seeded at a concentration of 2×10^4 in each well of 96-well plates and cultured overnight. Then, CA4P was added to the 96-well plates at different concentrations. The proliferation of the cells was measured using the CCK8 assay at the indicated time points. The CCK8 test was carried out according to the manufacturer's instructions (Mei5 Biological Company, China). The absorbance of each well was measured with a microplate reader at dual wavelengths of 450 nm and 690 nm.

Animal Experiments

We detected the antitumor effect of CAR-T cell therapy combined with CA4P on subcutaneous CDX models and PDX models. In the CDX model, SKOV3 (HER2⁺) cells representing ovarian tumors were subcutaneously injected into severe combined immunodeficient NPG mice. The PDX models were established with tissue derived from HER2⁺ colorectal or Meso⁺ ovarian cancer patients.[28] Further experiments were carried out when the size of the tumor was approximately 50 or 150 mm³. Approximately 2 weeks after tumor cell injection, normal T or CAR-T cells were injected into mice via the tail vein. For the groups treated with the combined therapy or CA4P alone, CA4P was intraperitoneally injected into mice at a dose of 100 mg/kg 4–6 h before T/CAR-T cell infusion. Posttreatment assessments were performed twice a week via flow cytometry, tumor-infiltrating lymphocyte (TIL) detection, peripheral blood tests, and TUNEL staining. Tumor burdens were monitored weekly using the Xenogen IVIS (Caliper Life Sciences). Tumor volumes were calculated with the following formula: V = ¹/₂(length × width2). Mice with large tumor masses were euthanized early because of humanitarian considerations. The protocols were approved by the Ethical Committee of Peking University Health Science Center.

Histology, Immunohistochemistry, and TUNEL Staining Analyses

Tissue specimens were fixed with 10% formalin, dehydrated with ethanol, and embedded in paraffin. The tissue samples were sliced into 4-μm-thick continuous sheets. The tissue sections were stained with H&E. Immunohistochemical staining was carried out by the streptavidin peroxidase method according to the manufacturer's instructions (Fuzhou Maixin Biotechnology Development Company, China). The expression levels of HER2, Meso, CD31, CD3, PD-L1, and Ki-67 were detected by immunohistochemistry. Microtubules were stained with a mouse anti-β-tubulin antibody. All antibodies were purchased from Abcam. The protocols were performed according to the operation guide of immunohistochemistry. For immunohistochemistry, tissue samples were fixed with 4% paraformaldehyde and embedded with paraffin. These sections were subjected to antigen retrieval. Samples were then incubated with corresponding antibodies overnight at 4°C. The samples were washed with PBS and incubated with a horseradish peroxidase (HRP)-conjugated IgG antibody. Then, the samples were observed, and images were collected with an optical microscope (CX41-23C02; Olympus, Tokyo, Japan). TUNEL staining was used to evaluate apoptosis in the tissue samples. The staining was carried out according to the manufacturer's instructions (Yi Sheng Biological Company). Red fluorescence represents apoptotic cells, whereas blue fluorescence (DAPI staining) represents nuclei.

Statistical Analyses

The data obtained in this study are expressed as the average ± SD (x ± s). Data comparisons between two samples were tested by a Student's t test, and those among multiple samples were tested by ANOVA. The significant difference level was set at α = 0.05. This means a difference was significant when the p value was less than 0.05. The p values are generally represented as follows: *p < 0.05, **p < 0.01, and ***p < 0.001. Fluorescence-activated cell sorting (FACS) data were analyzed by FlowJo 7.6.1 software or BD FACSCalibur tools. In this study, GraphPad Prism5 was used to generate graphs and perform statistical analyses.

SUPPLEMENTAL INFORMATION

AUTHOR CONTRIBUTIONS

CONFLICTS OF INTEREST

The authors declare no competing financial interests

ACKNOWLEDGMENTS

REFERENCES

1. Davenport, A.J., Jenkins, M.R., Cross, R.S., Yong, C.S., Prince, H.M., Ritchie, D.S., Trapani, J.A., Kershaw, M.H., Darcy, P.K., and Neeson, P.J. (2015). CAR-T cells inflict sequential killing of multiple tumor target cells. Cancer Immunol. Res. *3*, 483–494.

2. Sadelain, M., Rivière, I., and Riddell, S. (2017). Therapeutic T cell engineering. Nature *545*, 423–431.

3. Yip, A., and Webster, R.M. (2018). The market for chimeric antigen receptor T cell therapies. Nat. Rev. Drug Discov. *17*, 161–162.

4. Hartmann, J., Schüßler-Lenz, M., Bondanza, A., and Buchholz, C.J. (2017). Clinical development of CAR T cells—challenges and opportunities in translating innovative treatment concepts. EMBO Mol. Med. *9*, 1183–1197.

5. Mirzaei, H.R., Rodriguez, A., Shepphird, J., Brown, C.E., and Badie, B. (2017). Chimeric antigen receptors T cell therapy in solid tumor: challenges and clinical applications. Front. Immunol. *8*, 1850.

6. Waldner, H. (2009). The role of innate immune responses in autoimmune disease development. Autoimmun. Rev. *8*, 400–404.

7. Beatty, G.L., and O'Hara, M. (2016). Chimeric antigen receptor-modified T cells for the treatment of solid tumors: defining the challenges and next steps. Pharmacol. Ther. *166*, 30–39.

8. Becker, J.C., Andersen, M.H., Schrama, D., and Thor Straten, P. (2013). Immune-suppressive properties of the tumor microenvironment. Cancer Immunol. Immunother. *62*, 1137–1148.

9. Kakarla, S., and Gottschalk, S. (2014). CAR T cells for solid tumors: armed and ready to go? Cancer J. *20*, 151–155.

10. Vignali, D., and Kallikourdis, M. (2017). Improving homing in T cell therapy. Cytokine Growth Factor Rev. *36*, 107–116.

11. Bergers, G., and Hanahan, D. (2008). Modes of resistance to anti-angiogenic therapy. Nat. Rev. Cancer *8*, 592–603.

12. Jayson, G.C., Hicklin, D.J., and Ellis, L.M. (2012). Antiangiogenic therapy—evolving view based on clinical trial results. Nat. Rev. Clin. Oncol. *9*, 297–303.

13. Carmeliet, P., and Jain, R.K. (2011). Molecular mechanisms and clinical applications of angiogenesis. Nature *473*, 298–307.

14. Potente, M., Gerhardt, H., and Carmeliet, P. (2011). Basic and therapeutic aspects of angiogenesis. Cell *146*, 873–887.

15. Siemann, D.W., Bibby, M.C., Dark, G.G., Dicker, A.P., Eskens, F.A., Horsman, M.R., Marmé, D., and Lorusso, P.M. (2005). Differentiation and definition of vascular-targeted therapies. Clin. Cancer Res. *11*, 416–420.

16. Shojaei, F. (2012). Anti-angiogenesis therapy in cancer: current challenges and future perspectives. Cancer Lett. *320*, 130–137.

17. Woods, J.A., Hadfield, J.A., Pettit, G.R., Fox, B.W., and McGown, A.T. (1995). The interaction with tubulin of a series of stilbenes based on combretastatin A-4. Br. J. Cancer *71*, 705–711.

18. Grosios, K., Holwell, S.E., McGown, A.T., Pettit, G.R., and Bibby, M.C. (1999). In vivo and in vitro evaluation of combretastatin A-4 and its sodium phosphate prodrug. Br. J. Cancer *81*, 1318–1327.

19. Vincent, L., Kermani, P., Young, L.M., Cheng, J., Zhang, F., Shido, K., Lam, G., Bompais-Vincent, H., Zhu, Z., Hicklin, D.J., et al. (2005). Combretastatin A4 phosphate induces rapid regression of tumor neovessels and growth through interference with vascular endothelial-cadherin signaling. J. Clin. Invest. *115*, 2992–3006.

20. Badn, W., Kalliomäki, S., Widegren, B., and Sjögren, H.O. (2006). Low-dose combretastatin A4 phosphate enhances the immune response of tumor hosts to experimental colon carcinoma. Clin. Cancer Res. *12*, 4714–4719.

21. Sjögren, H.O. (1997). Therapeutic immunization against cancer antigens using genetically engineered cells. Immunotechnology *3*, 161–172.

22. Dark, G.G., Hill, S.A., Prise, V.E., Tozer, G.M., Pettit, G.R., and Chaplin, D.J. (1997). Combretastatin A-4, an agent that displays potent and selective toxicity toward tumor vasculature. Cancer Res. *57*, 1829–1834.

23. Tozer, G.M., Prise, V.E., Wilson, J., Locke, R.J., Vojnovic, B., Stratford, M.R., Dennis, M.F., and Chaplin, D.J. (1999). Combretastatin A-4 phosphate as a tumor vascular-targeting agent: early effects in tumors and normal tissues. Cancer Res. *59*, 1626–1634.

24. Siemann, D.W. (2011). The unique characteristics of tumor vasculature and preclinical evidence for its selective disruption by tumor-vascular disrupting agents. Cancer Treat. Rev. *37*, 63–74.

25. Sun, Q., Zhou, S., Zhao, J., Deng, C., Teng, R., Zhao, Y., Chen, J., Dong, J., Yin, M., Bai, Y., et al. (2018). Engineered T lymphocytes eliminate lung metastases in models of pancreatic cancer. Oncotarget *9*, 13694–13705.

26. Yu, S., Li, A., Liu, Q., Li, T., Yuan, X., Han, X., and Wu, K. (2017). Chimeric antigen receptor T cells: a novel therapy for solid tumors. J. Hematol. Oncol. *10*, 78.

27. Pan, J.H., Zhou, H., Cooper, L., Huang, J.L., Zhu, S.B., Zhao, X.X., Ding, H., Pan, Y.L., and Rong, L. (2019). LAYN is a prognostic biomarker and correlated with immune infiltrates in gastric and colon cancers. Front. Immunol. *10*, 6.

28. Teng, R., Zhao, J., Zhao, Y., Gao, J., Li, H., Zhou, S., Wang, Y., Sun, Q., Lin, Z., Yang, W., et al. (2019). Chimeric antigen receptor-modified T cells repressed solid tumors and their relapse in an established patient-derived colon carcinoma xenograft model. J. Immunother. *42*, 33–42.

29. Zhang, X., Zeng, Y., Qu, Q., Zhu, J., Liu, Z., Ning, W., Zeng, H., Zhang, N., Du, W., Chen, C., and Huang, J.A. (2017). PD-L1 induced by IFN-γ from tumor-associated macrophages via the JAK/STAT3 and PI3K/AKT signaling pathways promoted progression of lung cancer. Int. J. Clin. Oncol. *22*, 1026–1033.

30. Abiko, K., Matsumura, N., Hamanishi, J., Horikawa, N., Murakami, R., Yamaguchi, K., Yoshioka, Y., Baba, T., Konishi, I., and Mandai, M. (2015). IFN-γ from

lymphocytes induces PD-L1 expression and promotes progression of ovarian cancer. Br. J. Cancer 112, 1501–1509.

31. Eyquem, J., Mansilla-Soto, J., Giavridis, T., van der Stegen, S.J., Hamieh, M., Cunanan, K.M., Odak, A., Gönen, M., and Sadelain, M. (2017). Targeting a CAR to the TRAC locus with CRISPR/Cas9 enhances tumour rejection. Nature 543, 113–117.

32. Shum, T., Omer, B., Tashiro, H., Kruse, R.L., Wagner, D.L., Parikh, K., Yi, Z., Sauer, T., Liu, D., Parihar, R., et al. (2017). Constitutive signaling from an engineered IL7 receptor promotes durable tumor elimination by tumor-redirected T cells. Cancer Discov. 7, 1238–1247.

33. Martinez, M., and Moon, E.K. (2019). CAR T cells for solid tumors: new strategies for finding, infiltrating, and surviving in the tumor microenvironment. Front. Immunol. 10, 128.

34. Chinnasamy, D., Yu, Z., Theoret, M.R., Zhao, Y., Shrimali, R.K., Morgan, R.A., Feldman, S.A., Restifo, N.P., and Rosenberg, S.A. (2010). Gene therapy using genetically modified lymphocytes targeting VEGFR-2 inhibits the growth of vascularized syngenic tumors in mice. J. Clin. Invest. 120, 3953–3968.

35. Huang, Y., Yuan, J., Righi, E., Kamoun, W.S., Ancukiewicz, M., Nezivar, J., Santosuosso, M., Martin, J.D., Martin, M.R., Vianello, F., et al. (2012). Vascular normalizing doses of antiangiogenic treatment reprogram the immunosuppressive tumor microenvironment and enhance immunotherapy. Proc. Natl. Acad. Sci. USA 109, 17561–17566.

36. Shrimali, R.K., Yu, Z., Theoret, M.R., Chinnasamy, D., Restifo, N.P., and Rosenberg, S.A. (2010). Antiangiogenic agents can increase lymphocyte infiltration into tumor and enhance the effectiveness of adoptive immunotherapy of cancer. Cancer Res. 70, 6171–6180.

37. Huang, Y., Goel, S., Duda, D.G., Fukumura, D., and Jain, R.K. (2013). Vascular normalization as an emerging strategy to enhance cancer immunotherapy. Cancer Res. 73, 2943–2948.

38. Wallin, J.J., Bendell, J.C., Funke, R., Sznol, M., Korski, K., Jones, S., Hernandez, G., Mier, J., He, X., Hodi, F.S., et al. (2016). Atezolizumab in combination with bevacizumab enhances antigen-specific T-cell migration in metastatic renal cell carcinoma. Nat. Commun. 7, 12624.

39. Jain, R.K. (2014). Antiangiogenesis strategies revisited: from starving tumors to alleviating hypoxia. Cancer Cell 26, 605–622.

40. Dickson, P.V., Hamner, J.B., Sims, T.L., Fraga, C.H., Ng, C.Y., Rajasekeran, S., Hagedorn, N.L., McCarville, M.B., Stewart, C.F., and Davidoff, A.M. (2007). Bevacizumab-induced transient remodeling of the vasculature in neuroblastoma xenografts results in improved delivery and efficacy of systemically administered chemotherapy. Clin. Cancer Res. 13, 3942–3950.

41. Carmeliet, P., and Jain, R.K. (2011). Principles and mechanisms of vessel normalization for cancer and other angiogenic diseases. Nat. Rev. Drug Discov. 10, 417–427.

42. Ferrara, N., and Adamis, A.P. (2016). Ten years of anti-vascular endothelial growth factor therapy. Nat. Rev. Drug Discov. 15, 385–403.

43. Carmeliet, P., and Jain, R.K. (2011). Molecular mechanisms and clinical applications of angiogenesis. Nature 473, 298–307.

44. Kanthou, C., and Tozer, G.M. (2002). The tumor vascular targeting agent combretastatin A-4-phosphate induces reorganization of the actin cytoskeleton and early membrane blebbing in human endothelial cells. Blood 99, 2060–2069.

45. Beauregard, D.A., Hill, S.A., Chaplin, D.J., and Brindle, K.M. (2001). The susceptibility of tumors to the antivascular drug combretastatin A4 phosphate correlates with vascular permeability. Cancer Res. 61, 6811–6815.

46. Sengupta, S., Eavarone, D., Capila, I., Zhao, G., Watson, N., Kiziltepe, T., and Sasisekharan, R. (2005). Temporal targeting of tumour cells and neovasculature with a nanoscale delivery system. Nature 436, 568–572.

47. Rustin, G.J., Shreeves, G., Nathan, P.D., Gaya, A., Ganesan, T.S., Wang, D., Boxall, J., Poupard, L., Chaplin, D.J., Stratford, M.R., et al. (2010). A phase Ib trial of CA4P (combretastatin A-4 phosphate), carboplatin, and paclitaxel in patients with advanced cancer. Br. J. Cancer 102, 1355–1360.

48. Lu, Y., Yang, W., Qin, C., Zhang, L., Deng, J., Liu, S., and Qin, Z. (2009). Responsiveness of stromal fibroblasts to IFN-γ blocks tumor growth via angiostasis. J. Immunol. 183, 6413–6421.

49. Kammertoens, T., Friese, C., Arina, A., Idel, C., Briesemeister, D., Rothe, M., Ivanov, A., Szymborska, A., Patone, G., Kunz, S., et al. (2017). Tumour ischaemia by interferon-γ resembles physiological blood vessel regression. Nature 545, 98–102.

Supplemental Information

The Vascular Disrupting Agent CA4P Improves

the Antitumor Efficacy of CAR-T Cells

in Preclinical Models of Solid Human Tumors

Changwen Deng, Jingjing Zhao, Shixin Zhou, Jiebin Dong, Jixiang Cao, Junshuang Gao, Yun Bai, and Hongkui Deng
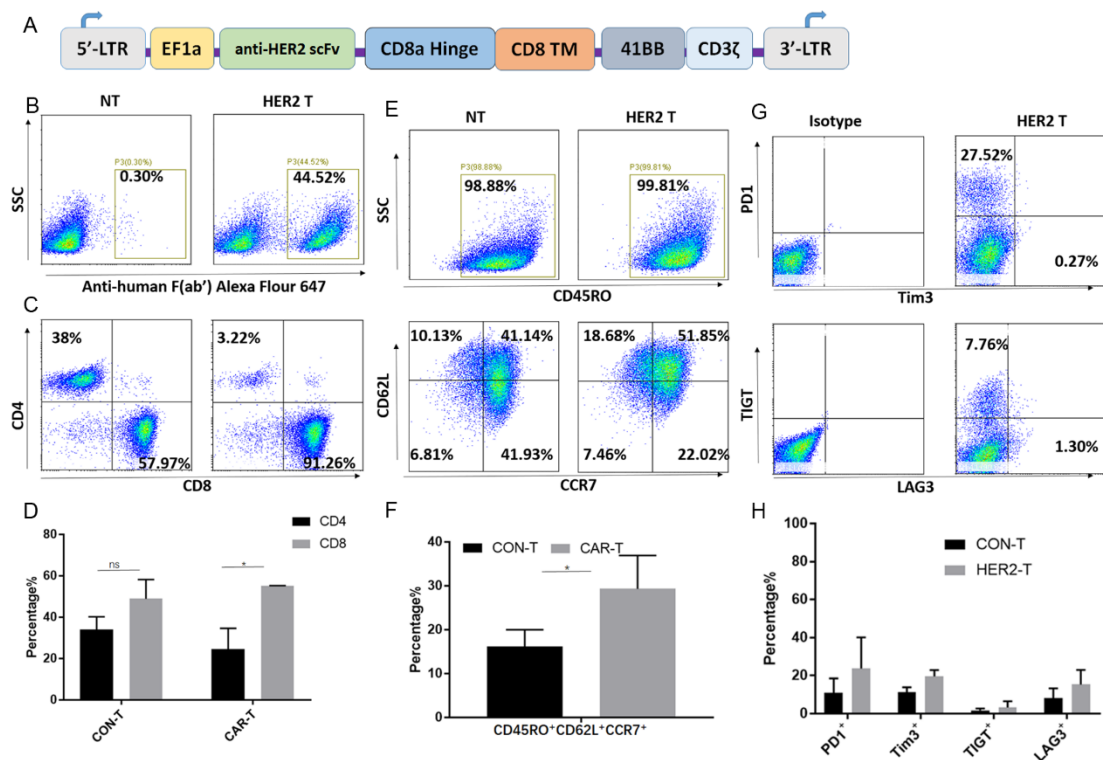
Supplemental Figure Legends

Figure S1. Construction and expression of a CAR to create HER2-CAR-T cells. (A) The structure of HER2-CAR comprised an Ig kappa signal peptide, an anti-HER2 (4D5) scFv, a CD8α hinge and transmembrane region, and a 4-1BB costimulatory signaling domain fused to the cytoplasmic region of the CD3ζ chain. This second-generation CAR was inserted into a self-inactivating (SIN) pRRL lentiviral vector with Xba I and Sal I sites. The expression of HER2-CAR was driven by the EF1-alpha promoter. (B) The expression of HER2-CAR in T cells was examined by flow cytometry with an Alexa Fluor 647-conjugated anti-human IgG, F(ab')2 antibody (BioLegend) 6 days after transduction. (C) The phenotypic subset composition of the CAR-T cell population was determined by flow cytometry 14 days after transduction. (D) The statistical analysis of the ratio of subset composition of the HER2-CAR-T cells in C generated from peripheral blood of three different donors (n=3).(E)The proportion of central memory T cells (CD45RO$^+$CCR7$^+$CD62L$^+$) was 51.85%, and the proportion in a control sample was 41.14%. (F) The statistical analysis of the ratio of central memory T cells of the HER2-CAR-T cells in E generated from peripheral blood of three different donors (n=3).(G) The proportions of HER2-CAR-T cells expressing exhaustion markers (PD1$^+$ 27.52%, LAG3$^+$ 1.3%, Tim3$^+$ 0.27%, and TIGT$^+$ 7.76%) were assayed by flow cytometry using appropriate antibodies (Biolegend) for flow cytometry analysis.(H) The statistical analysis of the proportions of HER2-CAR-T cells expressing exhaustion markers in G generated from peripheral blood of three different donors (n=3).
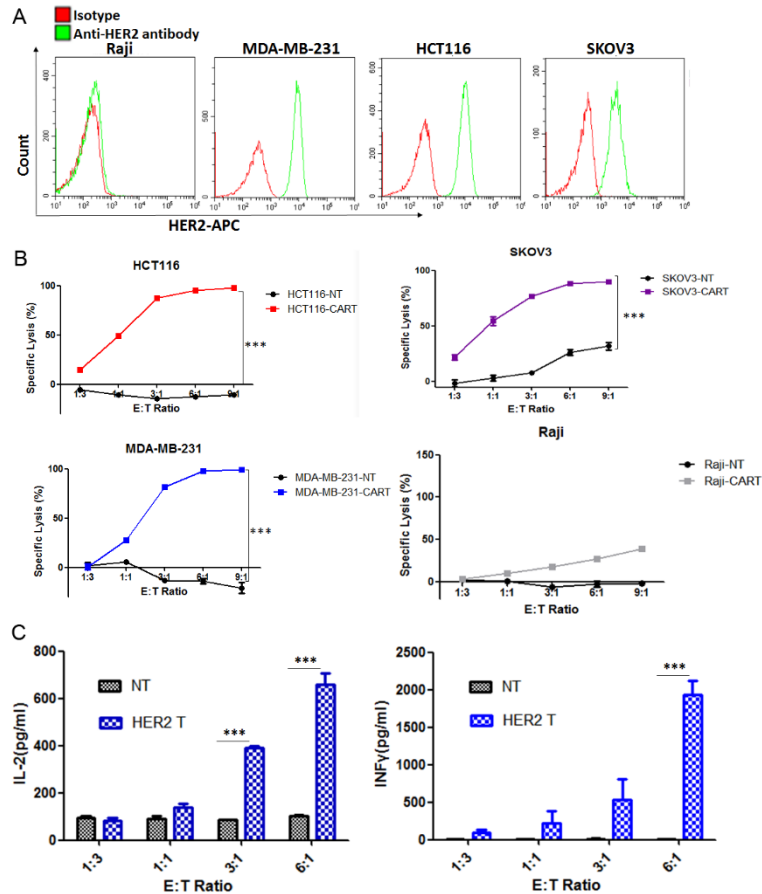
Figure S2. HER2-CAR-T cells kill target cells and secrete cytokines in a coculture system. HER2 antigen expression on the surface of tumor cells was determined by flow cytometry. (A) HER2 expression in the tumor cell lines HCT116 (colorectal cancer), SKOV3 (ovarian cancer), MDA-MB-231 (breast tumor) and Raji (lymphoma) was evaluated. (B) Normal T (NT) or CAR-T cells and HER2$^+$ or HER2$^-$ tumor cells were cocultured in a 96-well plate for 20 hours at the indicated effector-to-target (E:T) ratio, and then cytotoxicity was evaluated by a standard bioluminescence assay based on luciferase (n = 3, p < 0.001). (C) Normal T (NT) or CAR-T cells and HER2$^+$ SKOV3 tumor cells were cocultured in a 96-well plate for 24 hours at the indicated E:T ratio. The supernatants were collected, and an ELISA was used to determine the levels of secreted IL-2 and IFN-γ. The mean ± S.D. of triplicate cultures is shown (n = 3, p < 0.001).
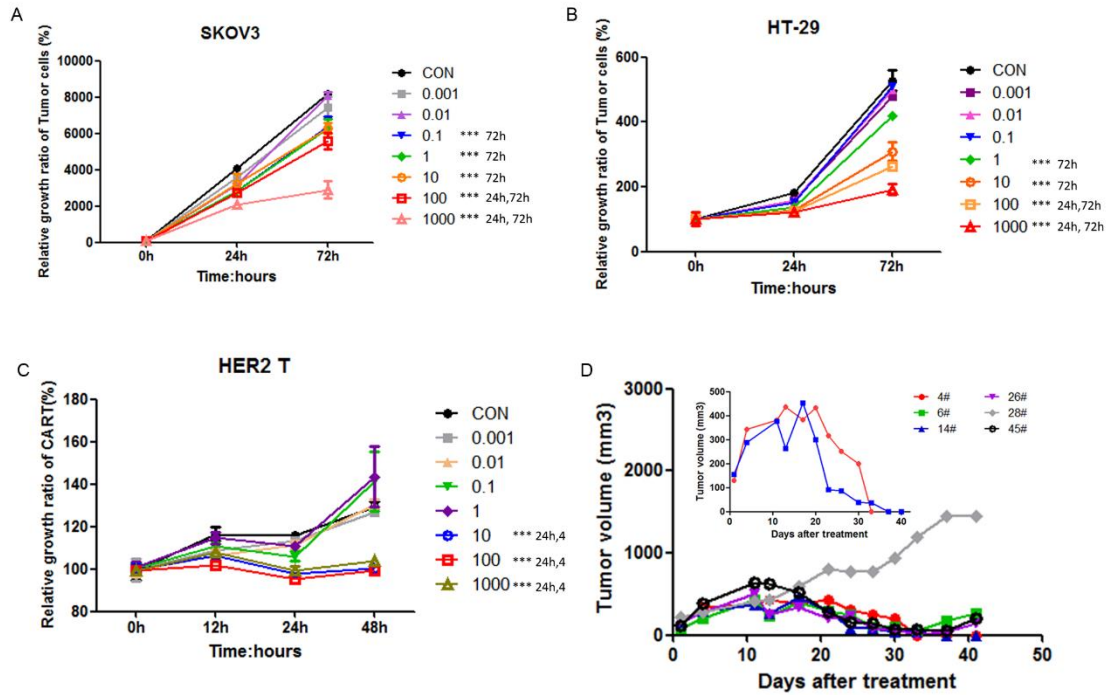
Figure S3. CA4P inhibits tumor cell, HER2-CAR-T cell proliferation. SKOV3 cells (A), HT29 cells (B), HER2-CAR-T cells (C) were seeded at a density of 2×10^4 cells in each well of 96-well plates and cultured overnight, with CA4P added at different concentrations(ng/ml). The proliferation of the cells was measured using a cell counting kit-8 (CCK-8) assay at the indicated time points. The absorbance of each well was measured with a microplate reader at dual wavelengths of 450 nm and 690 nm. All experiments were performed three times, and the results are presented as the mean ± standard deviation (ns, no significance; *, $p<0.05$; **, $p<0.01$; and ***, $p<0.001$; n ≥3).(D) SKOV3 cell-derived xenograft (CDX) model treated with HER2-CAR-T cells in combination with multiple CA4P treatments. Tumor growth curves of different groups. Compared with the other groups, the HER2-CAR-T cells combined with CA4P group showed significantly reduced tumor volumes (n=6, $p < 0.01$).Two (#4 and #14) of the 6 mice in the group showed complete tumor elimination.
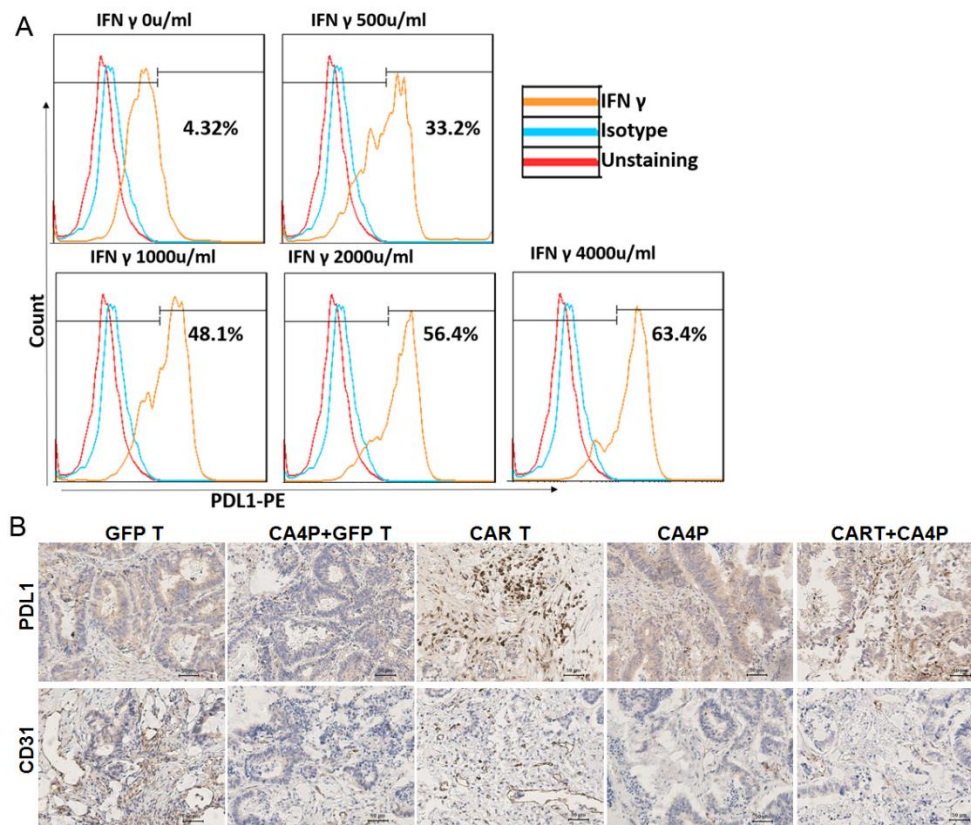
Figure S4. Effect of IFN-γ on the expression of PDL1 in tumors *in vivo* and PDL1 and CD31 expression in tumor tissue samples from patient-derived xenotransplantation (PDX) mouse models treated with HER2-CAR-T cells alone or in combination with CA4P. (A) Expression of PDL1 in SKOV3 cells induced by different concentrations of IFN-γ, as measured by flow cytometry. In total, 2×10^5 SKOV3 ovarian cancer cells were cultured in advance in a 6-well plate, and different concentrations of IFN-γ (5 concentrations between 0 and 4,000 U/ml) were selected. After 24 hours, the expression level of PDL1 was analyzed by flow cytometry, and the corresponding conditions were repeated three times. (B) PDL1 and CD31 expression in tumor tissue samples from PDX mouse models treated with HER2-CAR-T cells alone or in combination with CA4P. HER2-CAR-T cell (or GFP-T cell) infusions with or without CA4P treatments were carried out in PDX mouse models of HER2-positive colorectal cancer. Immunohistochemical analysis of the tumor tissue samples showed that PDL1 and CD31 expression differed among the GFP-T cells alone, CA4P alone, HER2-CAR-T cells alone, GFP-T cells combined with CA4P and CAR-T cells combined with CA4P groups (Scale bar, 50 μm).
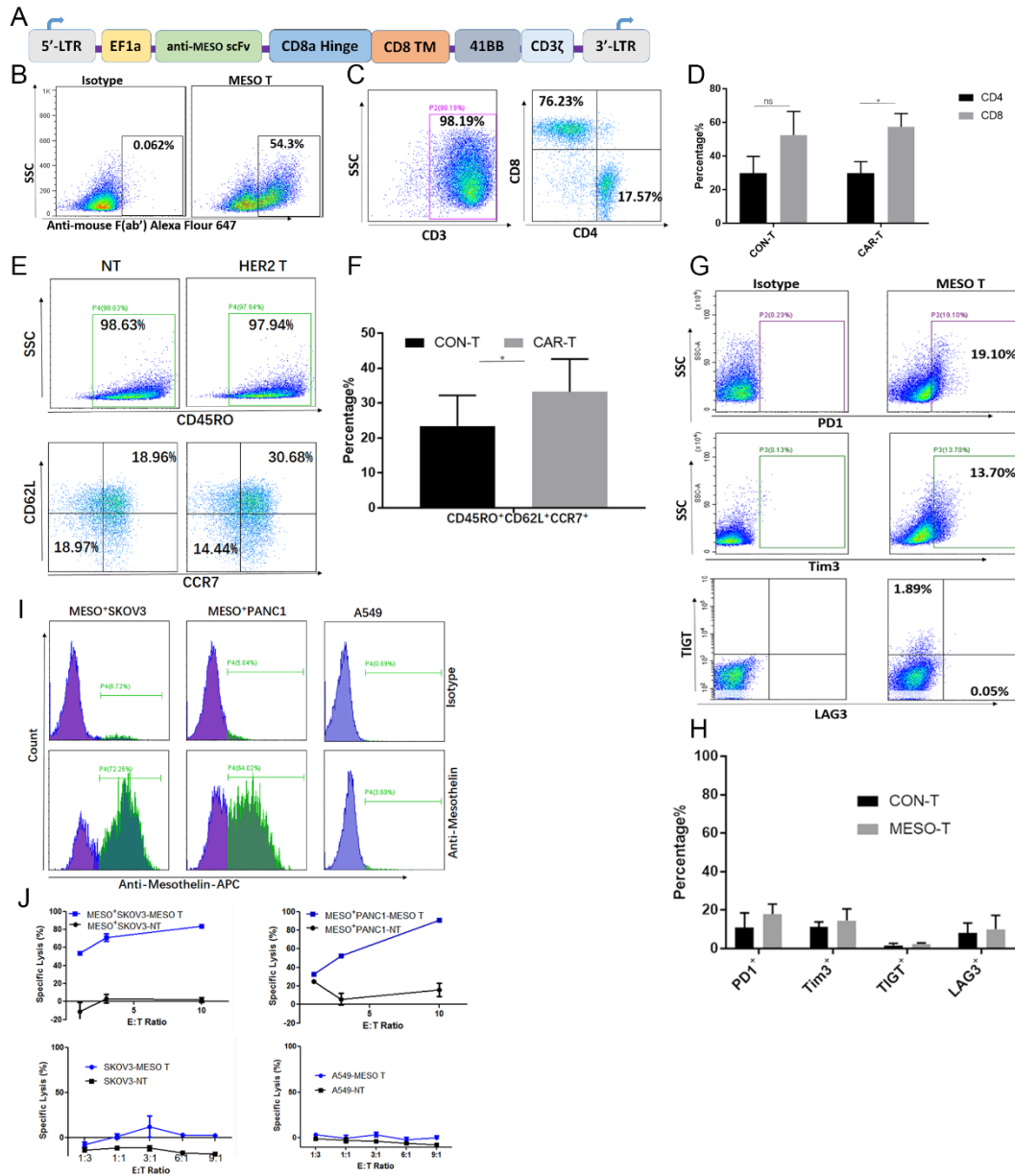
Figure S5. Construction, phenotype detection and cytotoxicity test of Meso-CAR-T cells. (A) The structure of Meso-CAR comprised an Ig kappa signal peptide, an anti-mesothelin (SS1) scFv, a CD8α hinge and transmembrane region, and a 4-1BB costimulatory signaling domain fused to the cytoplasmic region of the CD3ζ chain. (B) The expression of Meso-CAR in T cells was examined by flow cytometry with an Alexa Fluor 647-conjugated anti-mouse IgG, F(ab')2 antibody (BioLegend) 6 days after transduction. Approximately 54.3% of the T cells were CAR positive. The phenotypic subset composition of the CAR-T cell population was assayed by flow cytometry 14 days after transduction. (C) CD8+ T cells (76.23%) were dominant in the CAR-T cell population. (D)The statistical analysis of the ratio of subset composition of the Meso-CAR-T cells in C generated from peripheral blood of three different donors (n=3).(E)The proportion of central memory T cells (CD45RO+CCR7+CD62L+) was 30.68%, and the proportion in a control sample was 18.96%.(F) The statistical analysis of the ratio of central memory T cells in Meso-CAR-T cells generated from peripheral blood of three different donors performed using GraphPad Prism5 software compaired with the control T cells(n=3).

(G) The proportions of Meso-CAR-T cells expressing exhaustion markers (PD1$^+$ 19.10%, LAG3$^+$ 0.05%, Tim3$^+$ 13.7%, and TIGT$^+$ 1.89%) were assayed by flow cytometry using appropriate antibodies (Biolegend) for flow cytometry analysis.(H) The statistical analysis of the proportions of Meso-CAR-T cells expressing exhaustion markers in G generated from peripheral blood of three different donors (n=3).(I)To identify the functionality of the CAR-T cells *in vitro*, a lentiviral expression vector for high expression of the Mesothelin antigen was constructed, and then target cells(PANC1 and SKOV3) were transfected. The expression of the corresponding antigen was confirmed by flow cytometry. Mesothelin was overexpressed in the tumor cell lines MESO$^+$PANC1 and MESO$^+$SKOV3. (J)Normal T or CAR-T cells and Mesothelin$^+$ or mesothelin$^-$ tumor cells were cocultured in a 96-well plate for 20 hours at the indicated effector-to-target (E:T) ratio, and then cytotoxicity was evaluated by a standard bioluminescence assay based on luciferase (n =3, p< 0.001).